Tribological behavior of graphene nanoplatelet reinforced 3YTZP composites

F. Gutiérrez-Mora[1,2,*], A. Morales-Rodríguez[1,2], A. Gallardo-López[1,2], R. Poyato[1,2]

[1] Dpto. de Física de la Materia Condensada. Universidad de Sevilla. Apdo. 1065. 41080 Sevilla. Spain.

[2] Instituto de Ciencia de Materiales de Sevilla (CSIC-US). Américo Vespucio 49. 41092 Sevilla. Spain.

* Corresponding author. Tel. +34 954559977; email address: fegumo@us.es

Abstract

The tribological behavior of graphene nanoplatelet (GNP) reinforced 3 mol% yttria tetragonal zirconia polycrystals (3YTZP) composites with different GNP content (2.5, 5 and 10 vol%) was analyzed and discussed. Their dry sliding behavior was studied using a ball-on-disk geometry with zirconia balls as counterparts, using loads between 2 and 20 N at ambient conditions and compared to the behavior of a monolithic 3YTZP ceramic used as a reference material. The composites showed lower friction coefficients and higher wear resistance than the monolithic 3YTZP. An outstanding performance was achieved at 10 N, where the friction coefficient decreased from 0.6 to 0.3 and the wear rates decreased 3 orders of magnitude in comparison with the monolithic ceramic. A layer adhered to the worn surface was found for all the composites, but it did not acted as a lubricating film. The composites with the lowest GNP content showed an overall improved tribological behavior.

1. Introduction

Carbon-based nanomaterials, such as carbon nanotubes (CNTs) and graphene, have been proposed as ideal reinforcements for polymers, metals and ceramic matrices due to their small size, high aspect ratio and exceptional mechanical, electrical and thermal properties as well as their biocompatibility[1-6]. Their incorporation into different ceramic matrices has been extensively studied in the hope of obtaining tough, strong, electrically and thermally conductive materials. Various structural ceramics, like Al_2O_3, Si_3N_4 and ZrO_2, have been reinforced by CNTs and graphene-based fillers improving different properties, such as fracture toughness, thermal and electrical conductivities, for a detailed review see Ahmad et al[7].

Zirconia-based ceramics have a wide range of structural and functional applications in industry, including cutting tools, bearing parts, solid oxide fuel cells, oxygen sensors, ceramic membranes and medical prostheses owing to their excellent mechanical properties, good ionic conductivity and high temperature stability. Although the inherent brittleness of these materials limits their extensive use in applications where tribological aspects are involved, the use of CNTs[8,9] and graphene[10,11] as reinforcements has a positive impact in fracture toughness. Besides, carbon-based nanomaterials are prone to exhibit good lubricating properties due to the well-known behavior of graphite as a solid lubricant[12].

Despite the technological relevance of the wear behavior of these carbon-based nanomaterials zirconia composites, there are relatively few studies that deal with this problem, either with CNTs/zirconia composites[13-16] or graphene/zirconia materials[17]. Shin et al.[13] studied the tribological properties of fully dense yttria-stabilized zirconia (YSZ) reinforced with 1.0 wt% of single wall carbon nanotubes (SWCNTs). They found that, although the frictional behavior was unaffected by the incorporation of the carbon nanotubes, the wear resistance was noticeably improved, reducing the wear rate from 1.3×10^{-4} mm^3/Nm for YSZ to 9.6×10^{-6} mm^3/Nm for the composite. This improvement in wear resistance was associated with the corresponding improvement in fracture toughness. Shim et al.[14] studied composites of ZrO_2 with additions up to 9 vol% of multiwalled carbon nanotubes (MWCNTs). The friction coefficient (μ) showed the lowest value for the composite with 6 vol% of CNTs, with a moderate increment of this parameter for higher MWCNT content. The friction coefficient reduction (from 0.6 for the monolithic ceramic up to 0.25) occurred in composites with a significant level of

porosity (91-93% relative density). Denser materials (94-96% relative density) showed a more modest diminution in the friction coefficient (0.3 for the 3YTZP ceramic vs 0.25 for the composite with 6 vol% CNT addition) which was attributed to the suppression of crack formation and propagation at the contact zone. Similar results were obtained by Kasperski et al.[15] for zirconia with up to 5.16 wt% MWCNTs. They reported a 3.8-fold decrease (from 0.57 to 0.15) of the friction coefficient for the composite with 5.16 wt% carbon nanotubes with respect to yttria-stabilized zirconia, which was attributed to the formation of a lubricating film due to the exfoliation of the carbon nanotubes. Melk et al.[16] also reported the presence of such lubricating film in 3YTZP reinforced with up to 2 wt% MWCNTs on reciprocating friction tests. The effect of this layer was to decrease both the friction coefficient (from 0.85 to 0.57) and the wear rates (from 3×10^{-5} to $5x10^{-6}$ mm^3/Nm). To the best of our knowledge, only one study, carried out by Li et al.[17], has dealt with the tribological behavior of graphene based nanomaterial-reinforced zirconia, which reported the wear and friction behavior of a graphene nanosheet (1 wt% GNS) reinforced zirconia coating. These authors found a GNS-rich transfer layer on the wear tracks, which was more effective in reducing friction and wear at higher contact loads. At 100 N normal load, the friction coefficient was reduced from 0.27 for the monolithic sample to 0.19 for the composite. The wear rate of the composite was 1.17×10^{-6} mm^3/Nm, showing a 50% decrease from the value obtained for the monolithic 3YTZP.

Tribological studies using graphene as reinforcement in other ceramic bodies (mainly Al_2O_3 and Si_3N_4) are far more numerous[18-29]. In general, the incorporation of graphene to the composites improves their wear resistance and reduce their friction coefficient. Different mechanisms have been proposed to explain this behavior; such as the formation of a graphene-rich lubricating tribolayer due to the exfoliation of the embedded graphene platelets[18,23-29] or a graphene-induced fracture toughness improvement that positively affects the wear resistance[19,24].

In the present work, the tribological behavior of GNPs-reinforced zirconia composites is described. The friction and wear results of the composites are compared to the obtained ones from a monolithic 3YTZP ceramic used as a reference material. Energy-dispersive X-ray spectroscopy (EDX) and Raman spectroscopy analysis were performed to determine the nature of a transfer layer deposited on the wear track of the composites. To the best of our knowledge, this is the first study on the tribological properties of graphene nanoplatelets-reinforced bulk zirconia.

2. Experimental.

2.1. *Materials Processing.*

GNP/3YTZP composites with different GNP contents (2.5, 5 and 10 vol%) were prepared from 3 mol% yttria stabilized zirconia powder (40 nm particle size) supplied by Tosoh Corporation (Tokio, Japan) and graphene nanoplatelets from Angstron Materials (Dayton, Ohio, EEUU) with the following parameters: 50-100 nm average platelet thickness, 5 μm average lateral size, and 30 m^2/g specific surface area.

The ceramic powders were in a first place annealed at 850 ºC for 30 min in air. The nanoplatelets were dispersed in isopropyl alcohol, as it has been previously shown that this solvent assures a good GNP dispersion[30], and subjected to ultrasonic agitation by means of a high power ultrasonic probe (~750 W) (Model KT-600, Kontes Inc. Vineland, NJ) at 20 kHz and 95% amplitude applied for 15 min with 5 min cycles, refrigerating between cycles. After mixing with the ceramic powder, the suspensions were tip sonicated for 5 minutes. Drying of the suspensions was carried out on a hot plate while being stirred. Finally, the composite powders were homogenized in an agate mortar.

The composites were spark plasma sintered (Model 515S, SPS Dr Sinter Inc., Kanagawa, Japan) using a 15-mm diameter cylindrical graphite die/punch setup in vacuum atmosphere. A sheet of graphite paper was placed between the powders and the die/punches to ensure their electrical, mechanical and thermal contact. Graphitic paper was also placed along the circumference of the die for easy removal. The sintering processes were carried out at 1250 ºC with a holding time at peak temperature of 5 min, under a uniaxial pressure of 75 MPa. The heating and cooling rates were 300 and 50 ºC/min, respectively. For the sake of comparison, a monolithic 3YTZP ceramic was sintered in identical conditions. Sintered materials of 15 mm in diameter and ~ 3 mm in thickness were ground to eliminate the surface carbon.

The bulk densities were measured using the Archimedes' method, with distilled water as immersion medium. The theoretical density values for the composites were calculated by the rule of mixtures assuming density values of 6.10 g cm^{-3} for 3YTZP and 2.20 g cm^{-3} for GNPs.

2.2. *Microstructural characterization.*

Microstructural observations of the worn tracks were performed by high-resolution scanning electron microscopy (HRSEM), using a Teneo microscope (FEI, USA). This microscope was equipped with an X-ray energy dispersive spectrometer where chemical microanalysis on untested and worn areas of the composites was carried out.

Raman spectra of the composites before and after wear tests were recorded using a dispersive microscope (Horiba Jobin Yvon LabRam HR800, Kyoto, Japan) with Labsec 5.25.15 data acquisition software. The source was a 20 mW He–Ne green laser (532.14 nm). The microscope used a 600 lines per mm diffraction grid, a 100x objective and a confocal pinhole of 100 μm. The Raman spectrometer was calibrated using a silicon wafer. Six to eight spectra were acquired from each specimen. This spectroscopy was carried out in facilities belonging to the Instituto de Ciencia de Materiales de Sevilla (ICMS, CSIC-US).

2.3. *Mechanical and tribological characterization.*

Vickers indentation tests were carried out with a diamond Vickers microindenter (Duramin Struers, Germany) to establish the hardness at room temperature under 10 kgf, on samples polished up to 1 μm using diamond paste. At least 10 valid indentations were carried out on mirror-like finished surfaces for each sample, in well-separated and randomly selected regions on the surfaces latter subjected to wear testing. The hardness value, H_V (in GPa), was calculated from the indentation load, *P*, and the diagonal of the Vickers imprint, *a*:

$$H_V = 1.854(P/a^2)$$

Friction and wear tests were performed on a ball-on-disc tribometer (Microtest, Spain) to evaluate the tribological behavior of the fabricated samples. The tests were carried out using normal loads of 2, 5, 10 and 20 N and a sliding speed of 0.1 m/s at ambient air (40-60% relative humidity, room temperature) on polished surfaces (up to 1 μm using diamond paste, corresponding to surface roughness R_a below 0.01 μm). A zirconia ball 12.70 mm in diameter was used as a counterpart. The tests were stopped at a final sliding distance of 1000 m. The frictional force transferred to a load cell and the z-displacement of the center of the ball were recorded throughout the test. Each test was repeated at least twice for reproducibility. The wear rates and friction coefficients are

given as an average of the obtained results. The cross sectional area of the worn tracks was determined using confocal microscopy (DM3D, Leica, Germany) using at least 12 different profiles form different regions of each worn track. The wear rate (mm^3/Nm) was calculated using the following equation:

$$V = \frac{2\pi rS}{FL}$$

where r (mm) is the radius of the wear track, S the cross sectional area (mm^2) as determined by confocal microscopy, F the normal load (N) and L the sliding distance (m).

3. Results.

The microstructural features (density, grain size and GNP distribution) of the studied materials have been described elsewhere[31]. Briefly, all fabricated materials possessed densities near their theoretical values, and the composite materials showed grain sizes similar or slightly lower than the monolithic material (table 1). The values of the Vickers hardness are also presented in table 1. A decrease of H_v with increasing GNP content can be observed. This effect has been observed by different authors [18,31-34] and it has been related to the softer nature of the GNPs compared to the monolithic ceramic[32] and to GNP induced grain yielding and grain slipping[33,34]. Other authors have found an increase in hardness with increasing GNP content, but that effect was attributed to grain size refinement due to the graphene dispersion on the ceramic matrix rather than to any intrinsic effect of the GNPs on the hardness[35]. Typical curves representing the friction coefficient vs the sliding distance for a load of 10 N are shown in Fig. 1.a. Different behaviors can be observed in this plot for the different materials. The friction coefficients of both the monolithic material and the composite C2.5 show an almost constant steady-state value throughout all the test duration (0.65 and 0.25, respectively). On the other hand, the composites with a higher fraction of GNPs (C5 and C10) show a running-in period, marked by a sharp increment of μ. After this period, an intermediate regime characterized by a decrease of the friction coefficient before reaching the steady-state value can be observed. This intermediate regime extends for more than 200 m in C10. Then, a steady-state value of the friction coefficient is attained. A similar behavior, although much less marked, is visible for C5: a sharp peak

value of 0.31 followed by a decrease to 0.26 before reaching its steady state value of μ=0.29, similarly to the steady state friction coefficient for C10.

A similar trend is observed for all other loads. On the one hand, constant values of the friction coefficient for the monolithic ceramic and the C2.5 composite at low and intermediate loads ($\leq$10N) are found. On the other hand, a running-in stage, characterized by a sharp increase and a gradual reduction of the friction coefficient followed by an increase of μ until its steady-state value, is observed in C10 for all normal loads, in C5 for the tests performed at 10 and 20 N and also in C2.5 for 20 N normal load. This can be seen in Fig. 1.b, where the friction coefficient of the composite C10 is represented vs the sliding distance for different normal loads. The running-in characteristics are dependent on the test load. Namely, the sliding distances where the minimum value of both the friction coefficient and the steady-state friction coefficient are reached, decrease with load. For example, at 2 N neither the minimum nor the steady-state friction coefficient are attained within the duration of the tests (1000 m) while at 5, 10 and 20 N the minima occur at 625, 225 and 75 m, respectively.

The steady-state values of the friction coefficient obtained for the studied materials at the different loads are given in Fig. 2. These values of μ were calculated as the average over the last 200 m of each experiment, when a steady-state value was certainly attained. In certain tests, i.e. C10 composite at 2 N (Fig. 1.b), the friction coefficient did not reach any steady-state and consequently no value is presented in Fig. 2. The friction coefficient at normal loads higher than 5 N is lower for all composites when compared to the monolithic sample. In particular, the C2.5 composite shows a remarkable decrease of this parameter when compared to the 3YTZP ceramic (0.26 vs 0.7 at 5 N and 0.25 vs 0.65 at 10 N normal load). Focusing on the composites, the friction coefficient decreases when increasing the normal load for all compositions, being this variation more marked when the graphene phase content increases. For the C2.5 composite, μ varies from 0.29 at 2 N to 0.23 when tested at 20 N, while for the C5 composite, the variation is from 0.49 to 0.25, at 5 N and 20 N normal load, respectively. No tests were performed for monolithic 3YTZP at 20 N due to the possible deterioration of the testing equipment related to the mechanical vibrations associated to the high degree of wear of this sample.

Fig. 3 shows the wear rates of the monolithic 3YTZP ceramic and the composites for tests performed at 5, 10 and 20 N. Data for 2 N are not included as the topographic

studies performed using confocal microscopy revealed that the worn tracks on all samples tested under 2 N normal load were undetectable. Two facts can be inferred from this diagram: on the one hand, the wear rate for the monolithic 3YTZP is much higher than that of the composites, for example, at 10N the wear rate for the monolithic sample is almost three orders of magnitude higher than for C2.5 (1.4×10^{-5} vs 2.9×10^{-7} mm^3/Nm). On the other hand, the composites wear rates for a given normal load increases with the GNP content; with C2.5 showing the overall best wear resistance. In addition, the wear rates for a given composite increases with normal load (for example, for C2.5 from 2.9×10^{-7} mm^3/Nm at 5N to 4.5×10^{-7} mm^3/Nm at 20N).

Fig. 4 shows scanning electron micrographs of the wear tracks on 3YTZP ceramic (4.a) and C10 composite (4.b) tested under 5 N normal load. The wear damage in the C2.5 and C5 composites at this load level is almost undiscernible; only some plastic deformation grooves could be observed. The wear damage in the monolithic 3YTZP is typical of abrasive wear: brittle fracture particles produced due to tensile stresses on the contact zone were compacted to generate a heavily deformed surface. Plenty of loose debris was also found after the completion of the tests, further demonstrating that brittle fracture plays a major role on the wear mechanism of these samples. Severe wear could also be observed in C10 composite tested under the same normal load, although the wear rate is five times lower than in the monolithic ceramic (2.3×10^{-6} vs. 1.4×10^{-5} mm^3/Nm). Fig. 4.b shows a worn rough surface typical of brittle fracture. However, this surface is different from the one for the monolithic 3YTZP (Fig. 4.a), dark areas (indicated by arrows) are visible and a deposited layer is partially covering them. The roughness on this deposited layer is lower than on the bottom of the track indicating that it had been plastically deformed during the successive passes of the ball during the test. Grooves present on this layer are also an indication of plastic deformation.

Fig. 5 shows images of the worn tracks on the composites tested at 20 N. In these images, it can clearly be seen that the wear damage increases with the GNP content as it was quantitatively put forward in Fig. 3. Fig. 5.a shows that the wear damage in C2.5 composite is limited even at this load level, and that it is concentrated around the dark areas indicated by arrows. Fig. 5.b shows that the worn surface in C5 composite has the same features that the one in C10 composite tested at 5N (Fig. 4.b), namely a smooth deposited layer partially covering the rougher bottom of the track. The darker areas are also present in a higher proportion. Fig. 5.c shows that the presence of this deposited

layer in the C10 composite is residual, and most of the worn surface is produced by abrasive wear.

In order to elucidate the nature of the dark regions present on Fig. 4.b and Fig. 5, EDX analysis was performed on the C10 composite. The results shows that these dark regions present a higher amount of carbon than the rest of the surface (42±4 wt% C and 45±5 wt% Zr for dark region, and 25±5 wt% C and 65±5 wt% Zr for the rest of the surface).

The Raman study on the composites was performed before and after the tribological testing in order to analyse the GNP evolution during the wear tests and their role in the friction and wear behavior of the materials. Fig. 6 shows the Raman spectra acquired on the deposited layer and on the bottom of the worn track compared with the spectra obtained on the untested regions for all the composites. The characteristic D, G and 2D bands corresponding to the graphene stacks[36,37] are clearly observed in both untested and worn zones for all composites. The intensity ratio between D and G peaks is also included in the figures. This ratio can be used as an indication of the presence of defects in graphitic materials[30,38]. An increase of I_D/I_G is observed in all spectra acquired in the worn areas in comparison with the untested materials, accompanied by a slight growth of the D' peak which is also associated to defects. This increment is even higher for the deposited layer. In all the composites, similar values of I_D/I_G were obtained for similar regions, around 0.2 for the untested samples, 0.5 for the bottom of the worn track and 0.8 for the deposited layer. From these analyses, it is possible to affirm that the darker regions correspond to GNP clusters or agglomerations.

4. Discussion.

The friction and wear behavior of the monolithic zirconia in the whole range of normal loads used in this study can be described as severe wear regime (wear rates larger than 10^{-6} mm^3/Nm) according to the wear maps presented by Kato and Adachi[39]. Hvizdos et al.[40] have previously reported this wear regime for 3YTZP with similar experimental conditions. The wear mechanism is dominated by grain boundary fracture and grain pull-outs. The formation of a surface layer by severe plastic deformation and compaction of accumulated wear debris and subsequent delamination can also take place.

The composites friction coefficient is lower than that of the monolithic sample for normal loads higher than 5N, as it can be seen in figure 2. When comparing composites with different GNP content, the trend on μ with load could be explained using the hardness of the corresponding materials. It is a well-known fact that the friction coefficient increases when the hardness of one of the bodies intervening in the friction process decreases, while the hardness of the other body does not change[41]. This trend can be observed for 2 and 5 N normal load tests (Fig. 2), where the friction coefficient for C2.5 composite (H_V=13.0 GPa) is lower than for C5 composite (H_V=10.8 GPa). However, as the normal load increases, the steady-state friction coefficient for all the composites converges to a similar value. The explanation for this observation can be found in Fig. 1.b, where the evolution of the friction coefficient for the composite C10 with sliding distance at different loads is shown. For this composite, two friction regimes are observed: an initial stage with a high value of μ (higher than for the other harder composites), due to the softer nature of the sample (H_V=6.6 GPa). As the sliding proceeded, a second mechanism can be distinguished, when the surface was worn and wear debris started playing an important role on the friction process, reducing the friction coefficient. This fact was analyzed by monitoring the z-position of the zirconia ball that acted as counterpart in the test (not shown) which gave us an indication of where the deterioration of the surface began – since an increase in the z-value means material removal from ball and sample. The data showed that while the friction coefficient remained constant the z-value did not change significantly. However, when μ started to decrease the z-value also decreased, indicating that some layer was being deposited on the worn surface. As expected, the duration of this initial stage, characterized by a high friction coefficient and low surface damage, decreased with normal load. This is because higher loads produced more damage on the surface and, consequently, foments the presence of the wear debris necessary for the low friction stage that takes place for the rest of the test. Once the friction coefficient stabilizes in its steady-state value, the z-value starts to increase moderately, indicating material removal.

For the C5 composite, the similar observed trend can be explained using the intermediate value of the hardness for this composite. Similarly to the C10 composite, an initial stage characterized by higher friction coefficient was observed (Fig. 1.a), although much shorter, at 10 and 20 N normal loads. The steady-state friction

coefficient takes an intermediate value between the one for the initial stage of the softer C10 composite and the value for the harder C2.5 composite. As observed in the C10 composite, the friction coefficient decreases with the damage level and, consequently, with the normal load.

For the C2.5 composite, μ is independent on the normal load due to the higher hardness, as it has been argued. An initial stage, similar to the one described above, is observed for tests performed under 20 N for this composite.

The wear rate of the GNP composites is lower than that of the monolithic sample for all the experimental conditions, as it can be observed in Fig. 3. The composite wear rate increases moderately with load and most notably with GNP content, as it has been found by Rutkowski et al.[22] and Zhang et al[27] in composites with other matrices. Rutkowski et al. [22] found that additions larger than 4 wt% GNP to Si_3N_4 led to an increase of the mass loss. Zhang et al. [27] explained the lower wear rates for Al_2O_3 with 0.5 vol% GNP when compared to Al_2O_3 with 5 vol% GNP using the fact that in the latter material the GNPs were poorly dispersed and agglomerated. They claimed that these agglomerations acted as defects that weaken the structure and induced fracture in the adjacent region[27]. Fig. 5.a, illustrates damage located near the GNP agglomerations (indicated by black arrows) in the C2.5 composite tested at 20 N, supporting the idea that a similar process is acting in our materials.

In spite of these differences with the GNP content, the wear mechanisms are similar for all GNP volume fractions and all experimental conditions. For normal loads below a certain level that depends on the GNP content, the friction coefficient is low and the wear rates are below 10^{-6} mm^3/Nm. This wear regime can be described as mild wear. The wear mechanism in this regime is characterized by microabrasion and plastic deformation. Fine grooves produced by these wear modes are clearly seen in Fig. 7.a, for the C2.5 composite tested at 10 N. A transient regime is observed at the beginning of the tests above this load level, which is distinguished by a higher friction coefficient and a moderate wear damage. The load level for the transition between these two regimes decreases with the GNP content (20 N for C2.5, 10 N for C5 and 2 N for C10 composites) and it is associated with the decreasing value of the composite hardness. Grain-boundary fracture and grain pull-outs taking place during the friction process in this regime produce debris. This debris forms a layer that partially covers the wear track (Fig. 4.b). This deposited layer was present in all composites and experimental

conditions (Fig. 5). EDX analysis showed that its chemical composition (25±5 wt% C and 55±5 wt% Zr) was similar to the composition of the untested sample and of the bottom of the worn track. In the same sense, Raman spectra taken at the bottom of the worn track in composites with different GNP content showed no significant differences, and spectra from deposited layers on different samples tested under different experimental conditions displayed similar features.

From the increase of the I_D/I_G ratio on the Raman analysis on the wear track, it could be signaled that the deposited layer presents more defective GNPs than the polished surface. However, this does not necessarily imply a damage suffered by the GNPs during the wear process, as a higher D band has also been related to a major contribution of exposed GNP edges[42,44]. Recently, Román-Manso et al[42] have published Raman maps of pristine GNPs in which it can be observed how the defects are mostly concentrated over the edge of the GNP. Therefore, the GNPs in the deposited layer could maintain their structural quality but with a higher exposition of the GNP edges in comparison with the GNPs in the untested materials.

In these composites, the deposited layer is not the reason for obtaining a low friction coefficient, as is has been argued by many authors[18,23-29] for different systems, since low friction is also obtained for experimental conditions where this layer is not predominant (i.e. the C2.5 composite at low loads). The low friction coefficient in this case is attributed to the presence of the GNPs embedded in the 3YTZP matrix, present both in the worn surface and in the deposited layer. Moreover, Kim et al.[21] have reported a similar reduction of the friction coefficient without the presence of a tribolayer for graphene/alumina nanocomposites. They argued that continuous exposition of new graphene surface from the graphene embedded in the ceramic matrix during the wear tests originated this reduction in the friction coefficient.

The retention of the deposited layer on the worn surface is related to the presence of graphene-based nanostructures, as it can be seen in detail in Fig. 7.b where a dark area (corresponding to a carbon-rich phase) appears between the worn track and the deposited layer. This carbonaceous film could be acting as a glue for this layer[44], reason why the wear rate of the composites with higher GNP content is not as high as the one found for the monolithic 3YTZP. This deposited layer acts partially protecting the worn surface from further wear loss. Because of the presence of this layer, the wear rates for the composites in this regime are in the range of 10^{-6} mm^3/Nm - 10^{-5} mm^3/Nm, and fall

within the transition from mild to severe wear, according to Kato and Adachi's wear maps[39].

Overall, the composite that shows the best tribological behavior is C2.5, marked by a low friction coefficient and mild wear for all experimental conditions. The tribological behavior of this composite makes it an excellent candidate for technological applications (cutting blades, valves and impellors, ceramic membranes, medical prostheses, etc.). As the GNP content increases, so does the wear rate. In our composites, the wear damage is related to GNP agglomeration and the role that these agglomerates play as fracture initiation points, as it was suggested by Zhang et al.[27] for Al_2O_3 composites. The higher the GNP content, the higher the GNP agglomeration[31] and, consequently, more damage is produced during the friction process, as it has been found in our materials.

5. Conclusions.

The tribological behavior of GNP reinforced 3YTZP composites with different GNP content (2.5, 5 and 10 vol%) has been studied. The obtained results lead to state the following conclusions:

- The composites show a better tribological behavior in comparison with the monolithic sample, showing lower friction coefficient and wear rates. Particularly, the composite with 2.5 vol% GNP presents a wear rate 300 times lower than the monolithic 3YTZP when tested using a 10 N normal load.
- In all the composites, for normal loads below a certain level, the friction coefficient depends inversely on hardness, and wear proceeds by microabrassion and plastic deformation (mild wear regime).
- For higher loads, the wear damage increases, proceeding by microfracture and grain pull-outs, while the friction coefficient remains low. The wear debris originated in this process produces a deposited layer partially covering the worn surface, which limits the degree of wear. The wear rates are in the transition from mild to severe wear regimes.

Acknowledgements

This work was supported by project MAT2015-67889-P financed by the Spanish Ministry of Economy and Competitiveness and the European Research and Development Fund (ERDF) program.

References

1. Iijima S, Brabec CH, Maiti A, Bernhole ZJ, Structural flexibility of carbon nanotubes, *J. Chem. Phys.* 1996;**104**:2089-92.
2. Ebbesen TW, Lezec HJ, Hiura H, Bennet JW, Ghaemi HF, Thio T, Electrical conductivity of individual carbon nanotubes, *Nature* 1996:**382**:54-6.
3. Ruoff RS, Lorents DC, Mechanical and thermal properties of carbon nanotubes, *Carbon* 1995;**33**:925-30.
4. Chen H, Muller MB, Gilmore KJ, Wallace GG, Li D, Mechanically strong, electrically conductive, and biocompatible graphene paper, *Adv. Mater.* 2008;**20**:3557-61.
5. Balandin AA, Thermal properties of graphene and nanostructured carbon materials, *Nat. Mater.* 2011;**10**:569-81.
6. Novoselov KS, Falko, VI, Colombo L, Gellert PR, Schwab MG, Kim K, A roadmap for graphene, *Nature* 2012;**490**:192-200.
7. Ahmad I, Yazdani B, Zhu Y, Recent advances on carbon nanotubes and graphene reinforced ceramics nanocomposites, *Nanomat.* 2015;**5**:90-114.
8. Mazaheri M, Mari D, Schaller R, Bonnefont G, Fantozzi G, Processing of yttria stabilized zirconia reinforced with multi-walled carbon nanotubes with attractive mechanical properties, *J. Eur. Ceram. Soc.* 2011;**31**:939-45.
9. R.K. Chintapalli, F. Garcia Marro, B. Milsom, M. Reece, M. Anglada, Processing and characterization of high-density zirconia–carbon nanotube composites, *Mater. Sci. Eng. A* 2012;**549**:50-9.
10. Shin JH, Hong SH, Fabrication and properties of reduced graphene oxide reinforced yttria-stabilized zirconia composite ceramics, *J. Eur. Ceram. Soc.* 2014;**34**:1297-302.
11. Jin DQ, Yu J, Fei C, Qiang S, Zhang LM, Plasma activated sintering and mechanical properties of graphene reinforced zirconia ceramics, *Rare Met. Mat. and Eng.* 2015;**44**:274-6.
12. Bollmann W, Spreadborough J, Action of graphite as a lubricant, *Nature*. 1960;**186**:29-30.
13. Shin JH, Hong SH, Microstructure and mechanical properties of single wall carbon nanotube reinforced yttria stabilized zircona ceramics, *Mater. Sci. Eng. A* 2012;**556**:382-7.

14. Shim DH, Jung SS, Kim HS, Cho H, Kim JK, Kim TG, Yoon SJ, Effect of carbon nanotubes on the properties of spark plasma sintered ZrO_2/CNT composites, *Arch. Metall. Mater.* 2015;**60**:1315-8.
15. Kasperski A, Weibel A, Alkattan D, Estournès C, Turq V, Laurent Ch, Peigney A, Microhardness and friction coefficient of multi-walled carbon nanotube-yttria-stabilized ZrO_2 composites prepared by spark plasma sintering, *Scr. Mater.* 2013;**69**:338-41.
16. Melk L, Rovira JJR, Anti ML, Anglada M, Coefficient of friction and wear resistance of zirconia-MWCNTs composites, *Ceram. Int.* 2015;**41**:459-68.
17. Li H, Xie Y, Li K, Huang L, Huang S, Zhao B, Zheng X, Microstructure and wear behavior of graphene nanosheets-reinforced zirconia coating, *Ceram. Int.* 2014;**40**:12821-9.
18. Belmonte M, Ramírez C, González-Julián J, Schneider J, Miranzo P, Osendi, MI, The beneficial effect of graphene nanofillers on the tribological performance of ceramics, *Carbon* 2013;**61**:431-5.
19. Hvizdos P, Duzsa J, Balazsi C, Tribological properties of Si_3N_4-graphene nanocomposites, *J. Eur. Ceram. Soc.* 2013;**33**:2359-64.
20. Porwal H, Tatarko P, Saggar R, Grasso S, Mani MK, Dlouhy I, Dusza J, Reece MJ, Tribological properties of silica-graphene nanoplatelet composites, *Ceram. Int.* 2014;**40**;12067-74.
21. Kim HJ, Lee SM, Oh YS, Yang YH, Lim YS, Yoon DH, Lee C, Kim JY, Ruoff RS, Unoxidized graphene/alumina nanocomposite: fracture and wear resistance effects of graphene on alumina matrix, *Sci. Rep.* 2014;**4**:5176.
22. Rutkowski P, Stobierski L, Zientara D, Jaworska L, Klimczyk P, Urbanik M, The influence of graphene additive on mechanical properties and wear of hot-pressed Si_3N_4 matrix composites, *J. Eur. Ceram. Soc.* 2015;**35**:87-94.
23. Gutiérrez-González CF, Smirnov A, Centeno A, Fernández A, Alonso B, Rocha VG, Torrecillas R, Zurutuza A, Bartolomé JF, Wear behavior of graphene/alumina composite, *Ceram. Int.* 2015;**41**:7434-8.
24. Nieto A, Zhao JM, Han YH, Hwang KH, Schoenung JM, Microscale tribological behavior and in vitro biocompatibility of graphene nanoplatelet reinforced alumina, *J. Mech. Behav. Biomed. Mater.* 2016;**61**:122-34.

25. Maros M, Németh AK, Károly Z, Bódis E, Maros Z, Tapaszto O, Balázsi K, Tribological characterization of silicon nitride/multilayer graphene nanocomposites produced by HIP and SPS technology, *Trib. Int.* 2016;**93**:269–81.
26. Llorente J, Román-Manso B, Miranzo P, Belmonte M, Tribological performance under dry sliding conditions ofgraphene/silicon carbide composites, *J. Eur. Ceram. Soc.* 2016;**36**;429-35.
27. Zhang C, Nieto A, Agarwal A, Ultrathin graphene tribofilm formation during wear of Al_2O_3–graphene composites, *Nanomat. Energy* 2016;**5**:1-9.
28. Tapaszto O, Balko J, Puchy V, Kun P, Dobrik G, Fogarassy Z, Horváth ZE, Dusza J, Balazsi K, Balazsi C, Tapaszto L, Highly wear-resistant and low friction Si_3N_4 composites by addition of graphene nanoplatelets approaching the 2D limit, *Sci. Rep.* 2017;**7**: 10087.
29. Gutiérrez-Mora F, Cano-Crespo R, Rincon A, Moreno R, Domínguez-Rodríguez A, Friction and wear behavior of alumina-based graphene and CNFs composites, *J. Eur. Ceram. Soc.* 2017;**37**:3805-12.
30. Ramirez C, Osendi MI, Characterization of graphene nanoplatelets-Si_3N_4 composites by Raman spectroscopy, *J. Eur. Ceram. Soc.* 2013;**33**;471–7.
31. Gallardo-López A, Márquez-Abril I, Morales-Rodríguez A, Muñoz A, Poyato R, Dense graphene nanoplatelet/yttria tetragonal zirconia composites: Processing, hardness and electrical conductivity, *Ceram. Int.* 2017;**43**:11743-52.
32. Nieto A, Huang L, Han YH, Schoenung JM, Sintering behavior of spark plasma sintered alumina with graphene nanoplatelet reinforcement, *Ceram. Int.* 2015;**41**:5926-36.
33. Ahmad I, Islama M, Abdo HS, Subhani T, Khalil KA, Almajid AA, Yazdani B, Zhu Y, Toughening mechanisms and mechanical properties of graphene nanosheet-reinforced alumina, *Mater. & Design* 2015;**88**:1234-43.
34. Vu DT, Han YH, Chen F, Jin DQ, Schoenung JM, Lee DY, Graphene nano-platelets reinforced ZrO_2 consolidated by spark plasma sintering, *Sci. Adv. Mater.* 2016;**8**:312-7.
35. Liu X, Fan YC, Li JL, Wang LJ, Jiang W, Preparation and mechanical properties of graphene nanosheet reinforced alumina composites, *Adv. Eng. Mater.* 2015;**17**:28-35.

36. Ferrari AC, Meyer JC, Scardaci V, Casiraghi C, Lazzeri M, Mauri F, Piscanec S, Jiang D, Novoselov KS, Roth S, Geim AK, Raman spectrum of graphene and graphene layers, *Phys. Rev. Lett.* 2006:**97**;187401.
37. Malard LM, Pimenta MA, Dresselhaus G, Dresselhaus MS, Raman spectroscopy in graphene, *Phys. Rep.* 2009:**473**;51-87.
38. Gallardo-López A, Morales-Rodríguez A, Vega-Padillo J, Poyato R, Muñoz A, Domínguez-Rodríguez A, Enhanced carbon nanotube dispersion in 3YTZP/SWNTs composites and its effect on room temperature mechanical and electrical properties, *J. All. Comp.* 2016;**682**:70-9.
39. Kato K, Adachi K, Wear of advanced ceramics, *Wear* 2002;**253**:1097-104.
40. Hvizdos P, Mestra A, Anglada M, Effect of heat treatment on wear damage mechanisms in 3Y-TZP ceramics, *Wear* 2010;**269**:26-30.
41. Bowden FP, Tabor D, The friction and lubrication of solids, *Oxford Univ. Press*, 1950.
42. Román-Manso B, Domingues E, Figueiredo FM, Belmonte M, Miranzo P, Enhanced electrical conductivity of silicon carbide ceramics by addition of graphene nanoplatelets, *J. Eur. Ceram. Soc.* 2015;**35**:2723–31.
43. Casiraghi C, Hartschuh A, Qian H, Piscanec S, Georgi C, Fasoli A, Novoselov KS, Basko DM, Ferrari AC, Raman spectroscopy of graphene edges, *Nano Lett.* 2009;**9**:1433-41.
44. Ahmad I, Islam M, Alharthi NH, Alawadhi H, Subhani T, Munir KS, Shah SI, Inam F, Zhu Y, Chemical and structural analyses of the graphene nanosheet/alumina ceramic interfacial region in rapidly consolidated ceramic nanocomposites, *J. Compos. Mater.* 2017;**52:**417–28.

Table 1

GNP content, relative density, grain size and hardness of the studied materials

Material	GNP content (vol%)	Relative density	Grain size (μm)	Hv (GPa)
3YTZP	0	100%	0.26±0.11	13.39±0.15
C2.5	2.5	100%	0.22±0.10	13.0±1.4
C5	5.0	99%	0.21±0.09	10.8±0.3
C10	10.0	100%	0.25±0.11	6.6±0.6

Figure captions

Figure 1: Friction coefficient vs. sliding distance for (a) the monolithic ceramic and the GNP composites tested at 10 N, and (b) the C10 composite at all normal loads.

Figure 2: Steady-state friction coefficient for all composites and all normal loads used in the tests.

Figure 3: Average wear rates under different loads for all composites.

Figure 4: Scanning electron micrographs of the wear tracks on a) 3YTZP and b) C10 tested under 5 N normal load.

Figure 5: Scanning electron micrographs of the worn tracks on composites tested at 20 N: a) C2.5, b) C5 and c) C10.

Figure 6: Raman spectra of the untested and worn surface acquired on the composites: a) C2.5, b) C5 and c) C10. I_D/I_G ratio has been included above each spectrum

Figure 7: a) Microgrooves typical of mild wear generated on the worn surface after a test performed at 10 N in C2.5. b) Detail of a typical worn track in the mild/severe regime showing two distinct areas, the bottom of the track and a deposited layer.

a

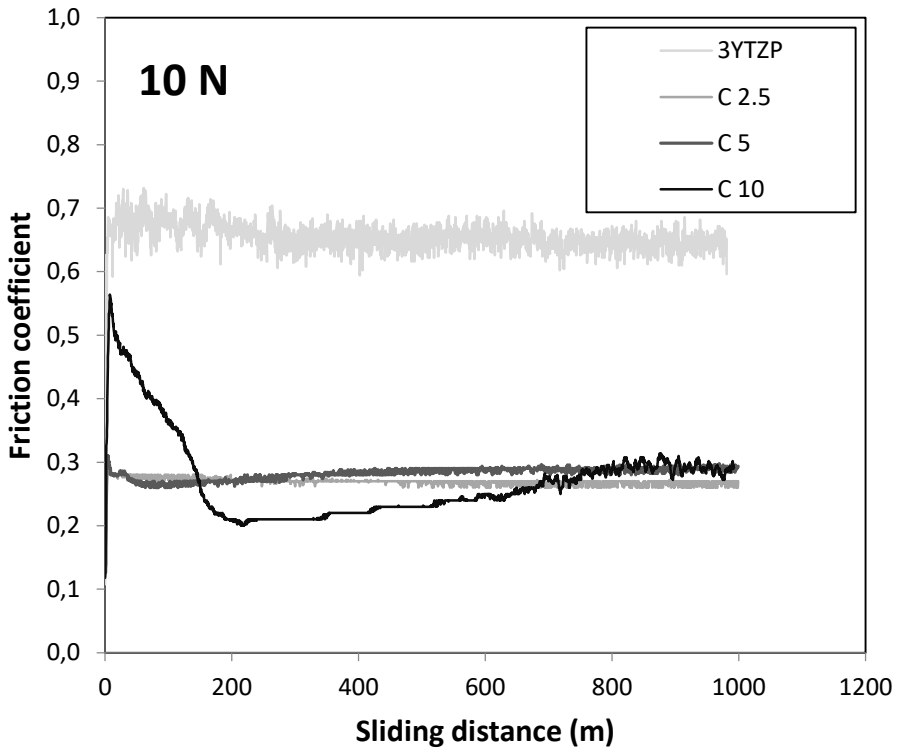
10 N
3YTZP
C 2.5
C 5
C 10
Friction coefficient
Sliding distance (m)
1,0
0,9
0,8
0,7
0,6
0,5
0,4
0,3
0,2
0,1
0,0
0
200
400
600
800
1000
1200

Figure 1.a

b

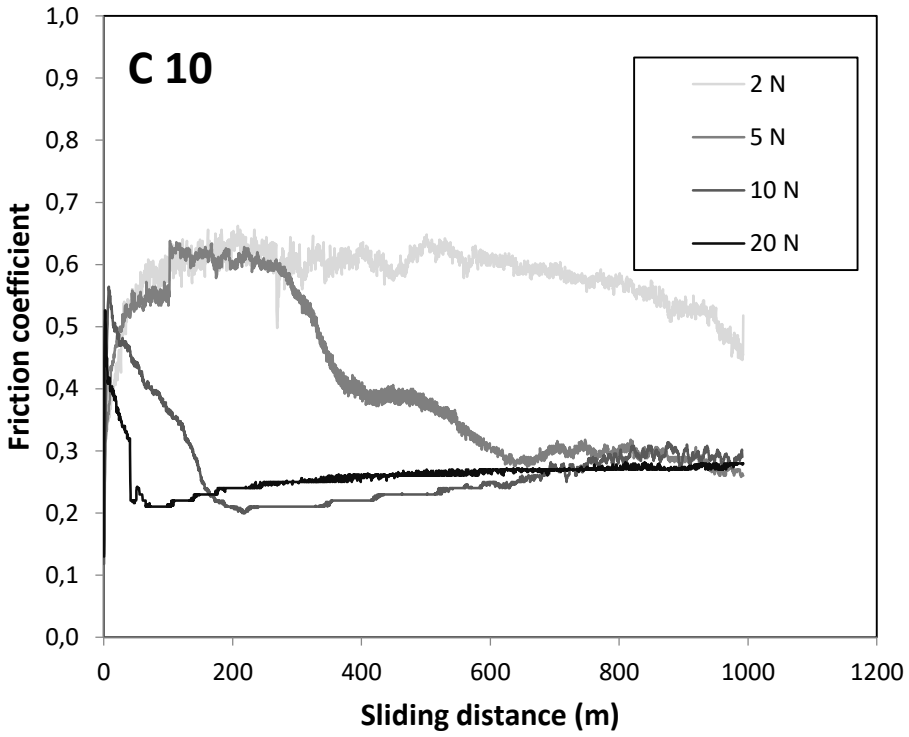
C 10
2 N
5 N
10 N
20 N
Friction coefficient
1,0
0,9
0,8
0,7
0,6
0,5
0,4
0,3
0,2
0,1
0,0
0
200
400
600
800
1000
1200
Sliding distance (m)

Figure 1.b

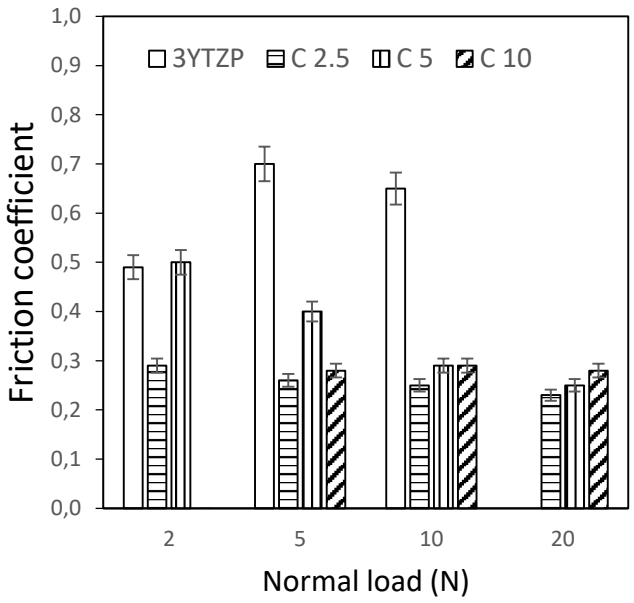
1,0
0,9
0,8
0,7
0,6
0,5
0,4
0,3
0,2
0,1
0,0
3YTZP
C 2.5
C 5
C 10
Friction coefficient
2
5
10
20
Normal load (N)

Figure 2

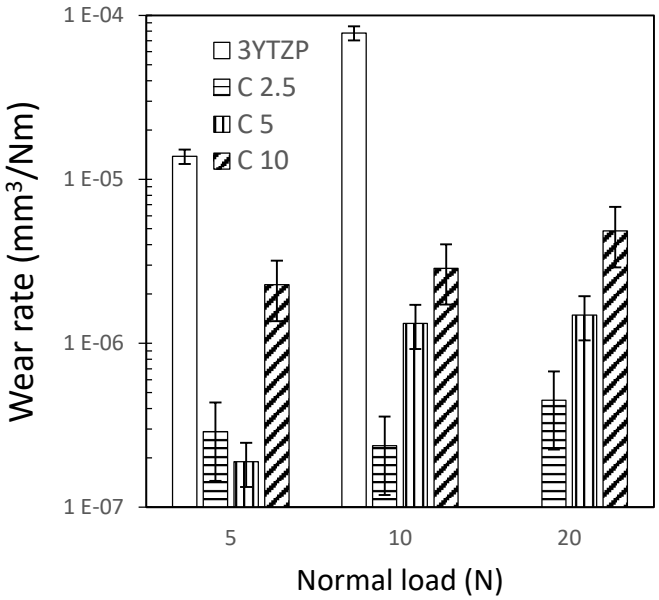
1 E-04
1 E-05
1 E-06
1 E-07
Wear rate (mm³/Nm)
3YTZP
C 2.5
C 5
C 10
5
10
20
Normal load (N)

Figure 3

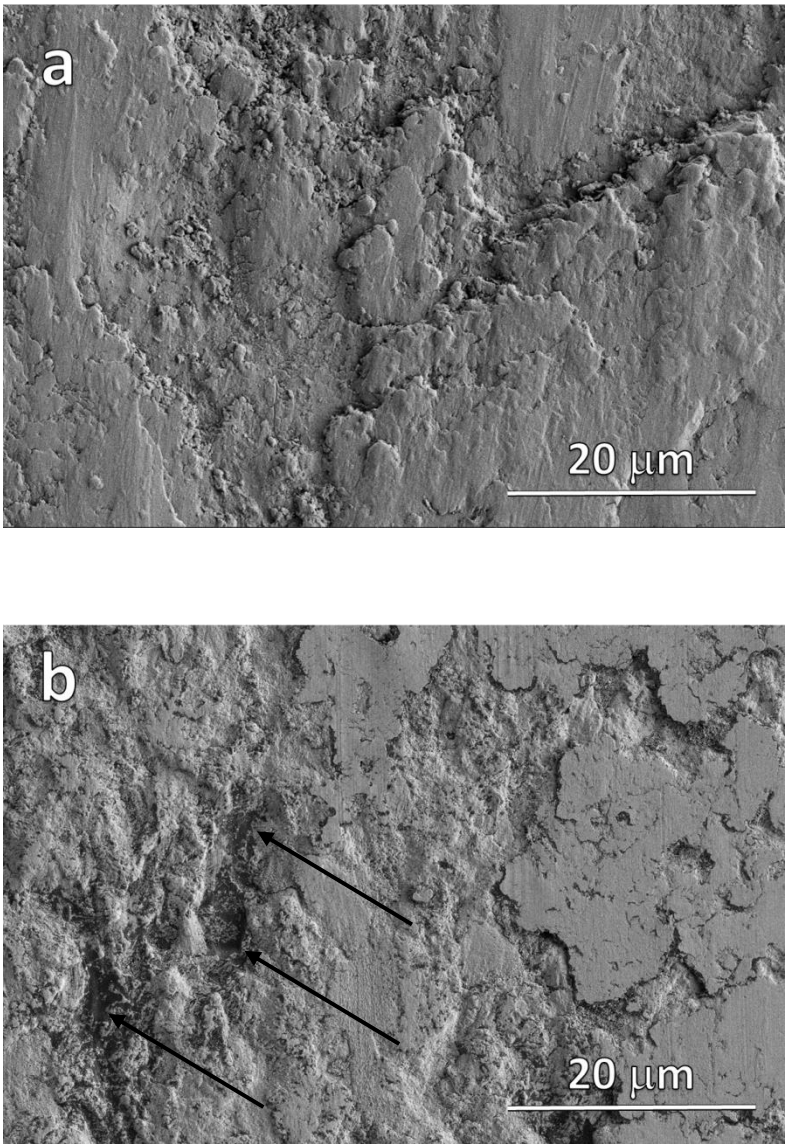

Figure 4

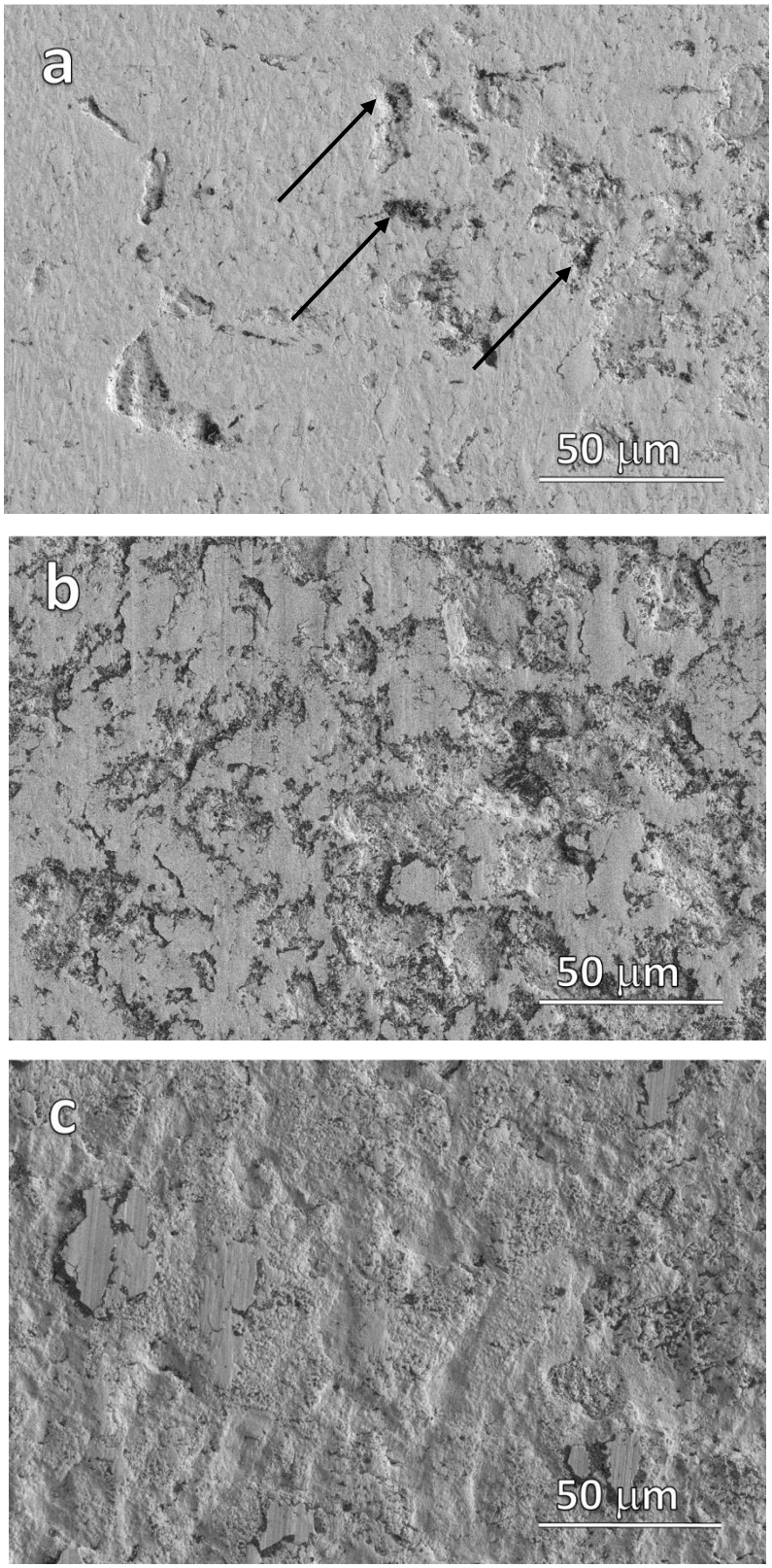

Figure 5

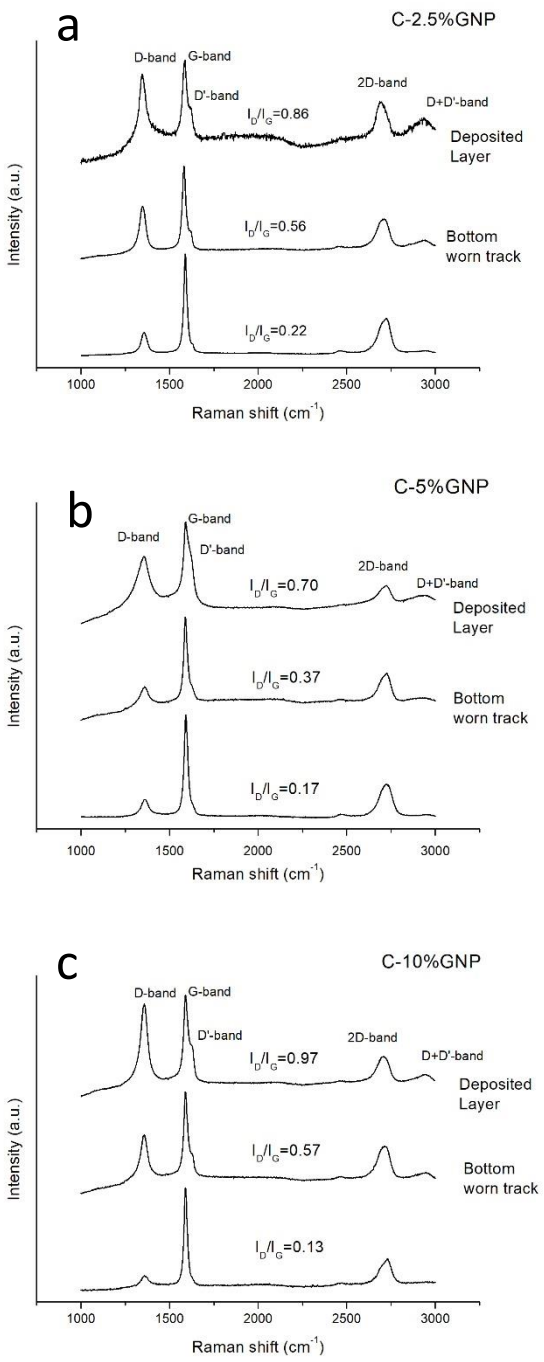
a
C-2.5%GNP
D-band
G-band
D'-band
2D-band
D+D'-band
I_D/I_G=0.86
Deposited Layer
I_D/I_G=0.56
Bottom worn track
I_D/I_G=0.22
Intensity (a.u.)
1000
1500
2000
2500
3000
Raman shift (cm^{-1})
b
C-5%GNP
D-band
G-band
D'-band
2D-band
D+D'-band
I_D/I_G=0.70
Deposited Layer
I_D/I_G=0.37
Bottom worn track
I_D/I_G=0.17
Intensity (a.u.)
1000
1500
2000
2500
3000
Raman shift (cm^{-1})
c
C-10%GNP
D-band
G-band
D'-band
2D-band
D+D'-band
I_D/I_G=0.97
Deposited Layer
I_D/I_G=0.57
Bottom worn track
I_D/I_G=0.13
Intensity (a.u.)
1000
1500
2000
2500
3000
Raman shift (cm^{-1})

Figure 6

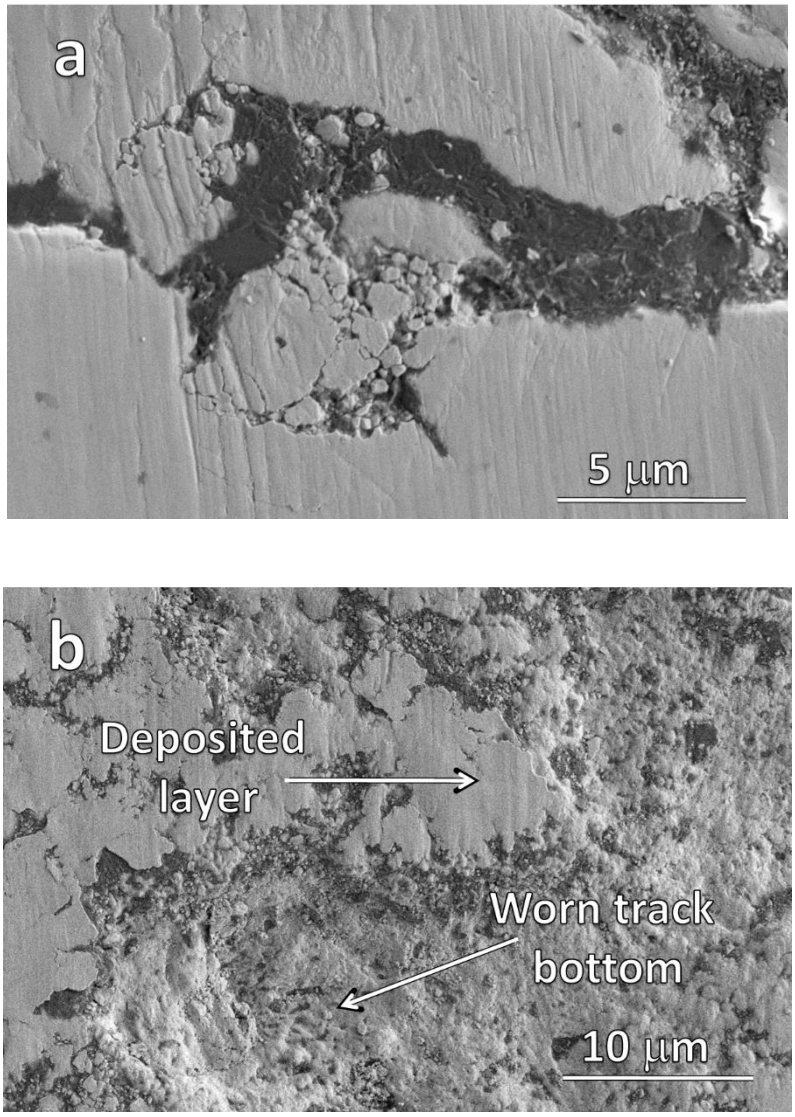

Figure 7